Developmental Biology 452 (2019) 43–54

Contents lists available at ScienceDirect

Developmental Biology

journal homepage: www.elsevier.com/locate/developmentalbiology

Temporal characterization of optic fissure basement membrane composition suggests nidogen may be an initial target of remodeling

Nicholas Carrara [1], Megan Weaver [1], Warlen Pereira Piedade [1], Oliver Vöcking, J.K. Famulski [*]

Department of Biology, University of Kentucky, USA

ARTICLE INFO

Keywords:
Basement membrane
Extracellular matrix
Nidogen
Coloboma
Retina
Optic fissure

ABSTRACT

Fusion of the optic fissure is necessary to complete retinal morphogenesis and ensure proper function of the optic stalk. Failure of this event leads to congenital coloboma, one of the leading causes of pediatric blindness. Mechanistically it is widely accepted that the basement membrane (BM) surrounding the maturing retina needs to be remodeled within the fissure in order to facilitate subsequent epithelial sheet fusion. However, the mechanism driving BM remodeling has yet to be elucidated. As a first step to understanding this critical molecular event we comprehensively characterized the core composition of optic fissure BMs in the zebrafish embryos. Zebrafish optic fissure BMs were found to express laminin a1, a4, b1a, c1 and c3, nidogen 1a, 1b and 2a, collagen IV a1 and a2 as well as perlecan. Furthermore, we observed that laminin, perlecan and collagen IV expression persists in the fissure during fusion, up to 56 hpf, while nidogen expression is downregulated upon initiation of fusion, at 36 hpf. Using immunohistochemistry we also show that nidogen is removed from the BM prior to that of laminin, indicating that remodeling of the BM is an ordered event. Lastly, we characterized retinal morphogenesis in the absence of nidogen function and documented retinal malformation similar to what is observed in laminin mutants. Taken together, we propose a model of BM remodeling where nidogen acts as a linchpin during initiation of optic fissure fusion.

1. Introduction

Development of vertebrates requires precise partitioning of developing tissues. This important function is bestowed on the outer covering of developing tissues, the basement membrane (BM). Located at the basal side of every epithelium, basement membranes play important roles in establishing and maintaining tissue borders, cell signaling, and providing biomechanical strength to physiologically active tissues. Comprised of various components specified to differing regions of the embryo, all BMs share a common core of 4 components including laminin, collagen IV, perlecan and nidogen (Yurchenco, 1990; Yurchenco and Schittny, 1990). Genomic comparisons conducted across numerous species have determined remarkable conservation of all four major basement membrane proteins even in distantly related phyla (Hutter et al., 2000; Hynes and Zhao, 2000). A critical aspect of BM biology during development involves their remodeling or dissociation, particularly during tissue fusion events. This is clearly apparent during the formation of the vertebrate retina, in particular fusion of the optic fissure. Upon the formation of a bi-layered optic cup, a fissure, the optic fissure, is formed in the ventral most region of the tissue. Serving as a conduit for endothelial cells to migrate and establish retinal vasculature, the fissure ultimately closes during an epithelial sheet fusion event to ensure a continuous and morphologically spherical structure of the retina (Barishak, 1992; Saint-Geniez and D'Amore, 2004). Failure of this fusion event leads to a congenital pediatric blinding disorder, coloboma, a leading cause of pediatric blindness (Chang et al., 2006; Stoll et al., 1997). Observed in several species, including zebrafish, chick and mouse, immunohistochemistry (IHC) of laminin clearly depicts a progressive removal of the BM during fissure fusion (Bernstein et al., 2018; Gestri et al., 2018; James et al., 2016). BM remodeling is therefore a critical component of the fusion process and it's failure is a likely culprit in the etiology of coloboma.

Coloboma has been the focus of scientific inquiry for well over a century, yet we still lack a general understanding of the molecular mechanism driving the fusion process. Major progress has been made in understanding the signaling and morphogenetic pathways that shape the fissure and subsequently signal for fusion. These pathways are known to involve Shh, BMP, TGFb and RA signaling in addition to several key

* Corresponding author.
E-mail address: jakub.famulski@uky.edu (J.K. Famulski).
[1] Indicates equal contribution.

https://doi.org/10.1016/j.ydbio.2019.04.012
Received 25 February 2019; Received in revised form 8 April 2019; Accepted 23 April 2019
Available online 26 April 2019
0012-1606/© 2019 Elsevier Inc. All rights reserved.

transcriptional regulators of fissure fusion such as vax1, vax2 and the best studied to date, pax2 (Hornby et al., 2003; Reis and Semina, 2015; Sanyanusin et al., 1995a; Sanyanusin et al., 1995b; Take-uchi et al., 2003; Gregory-Evans et al., 2004). However, we still lack a basic understanding of the molecular events that govern the physical fusion process. One such event undoubtedly involves the remodeling of the BM prior to fusion. Persistence of the BM presents as a physical barrier for fusion to occur and it is actually a hallmark of coloboma. Several coloboma models highlight the persistence of the BM as observed by laminin IHC (James et al., 2016; Liu et al., 2016; Tsuji et al., 2012). A key missing puzzle piece to our understanding of the molecular mechanisms driving fusion is therefore how and when does the BM undergo remodeling and subsequently removal from the fissure. To date only two ECM remodeling enzymes, MMP2 and ADAMTS16, have been associated with optic fissure fusion, however, their targets within the fissure have yet to be determined (Cao et al., 2018; Tsuji et al., 2018). Recent studies in several model organisms have elucidated the timing of fissure fusion by analyzing the removal of BMs as a readout for its initiation and its complete absence for its completion (Bernstein et al., 2018; James et al., 2016). Conclusions from these studies indicate an orderly progress of fusion originating at the most proximal region of the fissure, including the optic stalk and concluding at the distal most region of the optic cup. The molecular mechanisms involved in BM disassembly must therefore be regulated both temporally and regionally. Interestingly in all cases, laminin IHC was used to assess BM integrity. In fact, laminin is the only component of the BM that has been actively studied in regard to optic fissure fusion and/or BM remodeling (Lee and Gross, 2007; Parsons et al., 2002). While laminin is a critical component of the fissure it is only one of four core BM constituents. Furthermore, while laminin removal from the BM indicates that fusion is proceeding, it does not indicate how or when the remodeling started. It remains unknown whether BM core disassembly involves a step-wise process or occurs simultaneously. Examination of BM biology in other systems indicates that not all components are critical for assembly. Nidogen, for example, has been shown to be dispensable for BM assembly but is critical for its stability and rigidity (Aumailley et al., 1993). Collagen IV and laminin make up the bulk of the BM and are therefore also likely targets for remodeling. In addition, there are many matrix metalloprotease (MMP, ADAM, ADAMTS and cathepsin) enzymes known to be capable of targeting various components of the BM, but which have yet to be investigated during optic fissure fusion (Bonnans et al., 2014). Importantly, the exact composition of optic fissure BMs has yet to be defined. While collagen VI, laminin, nidogen and perlecan are expected to be represented in the optic fissure BM this has yet to be directly shown. Furthermore, each of the components, barring perlecan, is encoded by several orthologues and their expression has also not been examined in the context of fissure fusion. As such, we sought to fully characterize the molecular composition of the optic fissure BM during zebrafish retinal morphogenesis as the first logical step in deciphering the molecular mechanisms governing its remodeling.

Using whole mount *in situ* hybridization (WISH), we have confirmed the expression of perlecan and identified optic fissure expressed laminin, collagen IV and nidogen orthologues. In addition, we characterized their expression patterns throughout the process of fissure fusion. Interestingly, our findings indicate that the majority of BM components continue to be expressed well past the initiation of fissure fusion. Of note, we also observed that nidogen was the only component of the BM to be transcriptionally down regulated upon and during the initial stages of fissure fusion. Furthermore, when examining nidogen deposition in the fissure, we observed that nidogen was actively removed from the BM prior to that of laminin. Interestingly, this indicates that BM disassembly is an ordered event. Finally, we correlated nidogen loss of function with severe morphogenetic malformation of the optic cup and subsequent failure of optic fissure fusion.

2. Results

2.1. Optic fissure basement membrane comprises of laminin a1, a4, b1a, c1 and c3

Laminin is a heterotrimeric cross-shaped protein comprised of α, β, and γ chains (a, b and c hence forth) that plays roles in both BM structure and cell interaction via integrins (Aumailley, 2013). Genetic analyses have suggested that laminin provides the primary structural framework required for the recruitment and organization of other major BM components (Li et al., 2003). The terminal domain of laminin's long arm, the a chain, is responsible for both cell adhesion and self-assembly into polymers while the ends of laminin's short arms, b and c chains, are required for the formation of dimers and oligomers (reviewed in Aumailley (2013)). Previous examination of laminin gene family expression during zebrafish development indicated that majority of the alpha, beta and gamma subunits were expressed in the developing head and eye (Sztal et al., 2011). However, those studies did not focus on retinal anatomy or detailed pattern of expression. Analysis of laminin a1, b1 and laminin c1 expression and their corresponding mutant phenotypes, is to date the only direct examination of any BM gene expression in the optic fissure (James et al., 2016; Lee and Gross, 2007; Parsons et al., 2002). Laminin 111 is expected to be the predominant form of laminin heterodimers in the fissure, however this does not exclude the possibility of additional complexes. As such we sought to obtain a comprehensive outline of laminin gene expression during fissure fusion. To do so, we performed whole mount *in situ* hybridization (WISH) to track retinal expression of all 12 zebrafish laminin genes between 24 and 65hpf, spanning the course of fissure formation and fusion. Alpha chain laminin gene expression analysis included laminins a1, a2, a3, a4 and a5 (Fig. 1A). At 24hpf only laminin a1 and a4 display expression in the eye and in particular in the optic fissure (Fig. 1A, Fig. 1A). Similar expression patterns are observed at 48hpf. Laminin a2, a3 and a5 display varying expression throughout the cranial regions while laminin a5 is detected in the lens at 48hpf. Beta chain expression analysis included laminins b1, b1b, b2 and b4 (Fig. 1B). Only one beta chain laminin indicated expression in the optic fissure, laminin b1. Both 24 and 48hpf embryos clearly display laminin b1 signal in the fissure (Fig. 1B, Fig. S1A). Remaining laminin beta genes show weak expression in the cranial and periocular regions. Gamma chain laminins examined included laminin c1, c2 and c3 (Fig. 1C). Both laminin c1 and c3 display expression in the optic fissure at both 24 and 48hpf while laminin c2 expression appears to be epidermal at this stage of development (Fig. 1C, Fig. S1A).

Having established which laminin genes are expressed during optic fissure fusion, we next sought to determine whether their expression correlates to the initiation or completion of fissure fusion. Recent work has pinpointed the initiation of fissure fusion in zebrafish to commence at ~32-36hpf, actively fusing by 48hpf and mostly completed fusion by 72hpf (Bernstein et al., 2018; James et al., 2016). To precisely track timing of laminin expression during fissure fusion, we examined laminin expression at 24, 48, 56 and 65hpf (Fig. 1D). Isolated retinas imaged using DIC indicated that all 5 laminin genes were still expressed in the region of the fissure at 48hpf, while laminin c3 expression persisted until 56hpf. By 65hpf all of the laminin genes were no longer expressed in the fissure. Taken together, our results confirmed the expected expression of laminins a1, b1 and c1, in addition to uncovering laminin a4 and c3 as novel additions to the laminin repertoire included in optic fissure BMs. We also determined that laminin expression generally persists up to and including 48hpf, which is a time when fusion is actively occurring.

2.2. Perlecan expression in the optic fissure persists up to the conclusion fusion

Perlecan, the most prominent proteoglycan of the BM, consists of a 400–500 kDa (80 nm) core protein attached to three heparan sulfate and/or chondroitin sulfate chains (70 kDa-100kDa each) (Paulsson et al.,

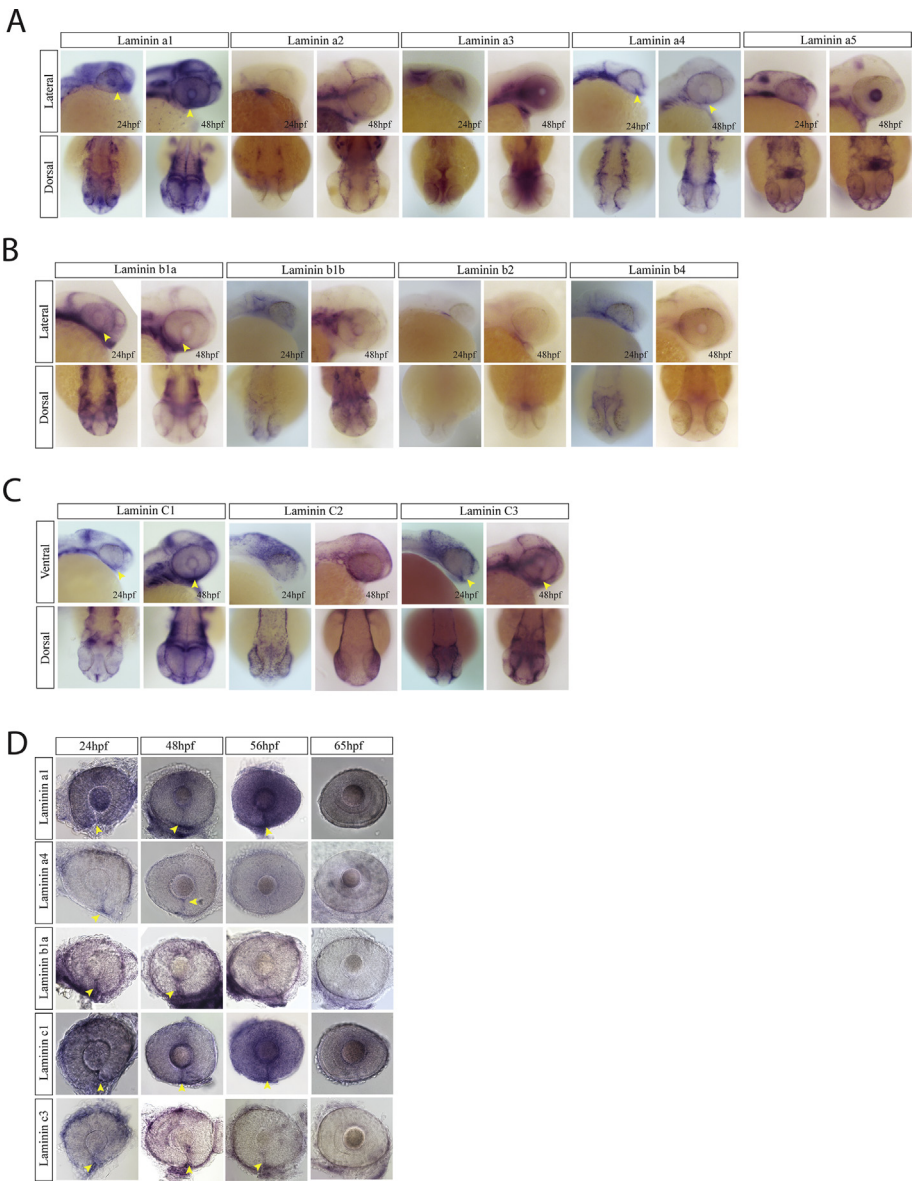

Fig. 1. Laminin expression during optic fissure formation and fusion. **A)** WISH for zebrafish laminin alpha chain genes a1, a2, a3, a4 and a5. Expression was analyzed at 24 and 48hpf and visualized in lateral and dorsal views. At 24 and 48hpf laminins a1, a4 and a5 were observed to express within the optic fissure (yellow arrow heads). Laminin a2 and a3 were largely absent from the retina while laminin a5 was expressed in the developing lens at 48hpf. **B)** WISH for laminin beta chain genes b1, b2 and b3 at 24 and 48hpf. Only laminin 1b was found to be expressed in the optic fissure (yellow arrow heads). Laminin b2 and b3 were largely absent from the retina. **C)** WISH for laminin genes c1, c2 and c3 at 24 and 48hpf. Laminin c1 and c3 were detected in the optic fissure (yellow arrow heads) while c2 appears to primarily be expressed in the ectoderm. **D)** WISH time course examination of laminin gene expression in the optic fissure. Laminin a4 and b1 are expressed in the fissure up to 48hpf, while a1, c1 and c3 retain expression up to 56hpf (yellow arrow heads).

1987; Timpl, 1993). It has been indicated as a key regulator of BM signaling (Smith et al., 2007). Zebrafish encode a single perlecan gene, hspg2, which was identified and characterized by Zoeller et al., in 2008 (Zoeller et al., 2008). Using WISH and IHC the authors showed that perlecan was expressed in the head, eye and somites. However, the authors did not focus their attention on retinal or optic fissure expression of perlecan. As such, we performed perlecan *in situ* hybridization at 24 hpf and observed a low level of expression in the optic fissure and periphery of the developing retina (Fig. 2A, Fig. S1B). By 48 hpf, perlecan is clearly expressed in the optic fissure and surrounding the forming lens (Fig. 2A, Fig. S1B). At 56hpf perlecan expression continues to outline the lobes of the fissure with a strong signal (Fig. 2B). Interestingly, at 65hpf, while perlecan expression is diminished it is still clearly observable as a single line of expression across where the fissure had fused. This suggests that on a transcriptional level, perlecan does not appear to be down regulated in anticipation of fissure fusion and or its mRNA persists in the fusing cells for an extended amount of time.

2.3. Collagen IV is represented in the optic fissure by col4a1 and col4a2

The second most abundant protein in the BM, collagen IV, encodes three functional domains a1, a2 and a globular domain NC1 at the carboxy-terminus (~550 kDa). Collagen IV's amino-terminus interacts with three other collagen IV proteins resulting in a characteristic chicken wire shaped quaternary assemblage (Brown et al., 2017). This uniquely shaped arrangement increases the elasticity of the matrix and ultimately its biomechanical strength. Col4a1 and 4a2 are predicted to be components of most BM, with other col4 genes exhibiting tissue and developmental variability in expression (Khoshnoodi et al., 2008). As we had previously done for laminin and perlecan, we sought to characterize the composition of the optic fissure BM by analyzing collagen IV expression. Zebrafish encode 6 collagen IV genes, col4a1-a6. Apart from col4a1 and col4a5 WISH images deposited to ZFIN, a search of the literature did not provide any significant results for analysis of collagen IV expression in early zebrafish. Therefore, we examined the expression of all 6 col4 genes using *in situ* hybridization at 24 and 48hpf with a focus on retinal and optic fissure expression (Fig. 3A). Upon analysis of our results we can conclude that all 6 genes had expression in the eye, with collagen 4a3-4a6 expression restricted to the periphery of the lens pit. On the other hand, col4a1 and col4a2 expression was absent from the lens region, but clearly present in the optic fissure (Fig. 3A, Fig. S1C). Col4a1 and col4a2 appear to also have overlapping expression throughout the

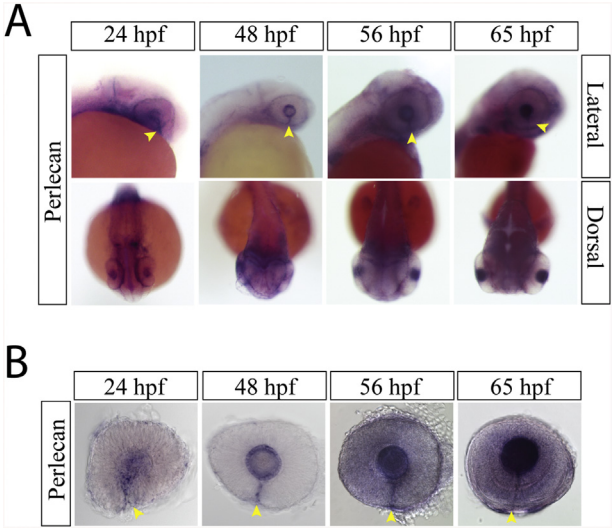

Fig. 2. Perlecan expression during optic fissure formation and fusion. **A)** WISH for zebrafish perlecan at 24, 48, 56 and 65hpf. Perlecan expression is observed in the lens and the optic fissure from 24 to 65 hpf (yellow arrow heads). **B)** Examining WISH in isolated zebrafish eyes at 24, 48, 56 and 65hpf indicates that perlecan expression persists in the optic fissure (yellow arrow heads) up to 65hpf.

head region (Fig. 3A). Having identified optic fissure associated collagen IV genes, we next tracked their expression patterns throughout optic fissure fusion. *In situ* analysis on isolated retinas indicates that both col4a1 and col4a2 expression persists until 56hpf and is largely absent from the region of the fissure by 65hpf (Fig. 3B). These findings run parallel with our analysis of laminin and perlecan gene expression, where although fusion is close to complete, these particular BM components continue to be expressed.

2.4. Nidogen 1a, 1b and 2a are expressed in the optic fissure

The final core component of the BM yet to be characterized for expression during optic fissure fusion is nidogen. Compared to the other BM core components, Nidogen is a relatively small BM protein (~150 Kd) comprised of three globular domains separated by two spacer regions. Nidogen's largest β-barrel shaped domain G2 has the ability to bind to both collagen IV and perlecan, while it's G3 domain binds to the γ chain of laminin (Aumailley et al., 1989, 1993; Chung and Durkin, 1990; Tsao et al., 1990). Similar to collagen IV and perlecan, little to no nidogen expression data from zebrafish embryos exists. Zebrafish encode 4 nidogen homologues, nid1a, 1b, nid2a and 2b and we therefore analyzed all 4 using WISH between 24 and 48hpf (Fig. 4A). To our knowledge, this is the first comprehensive examination of nidogen family expression in zebrafish embryos. Interestingly, all 4 nidogen orthologues display regions of unique expression patterns throughout the embryos, particularly in the tail and head regions. Nid1a is expressed throughout the somites while nid2a is expressed in the tail tip. Nid1a, 1b and 2a are all expressed in the head region and surrounding the eye between 24 and 48hpf. Furthermore, nid1a, 1b and 2a were all found to express in the optic fissure starting at 24hpf (Fig. 4A, Fig. S1D). Nid2b appears to be expressed at very low levels at 24hpf and further declines by 36 and 48hpf. We next correlated nidogen expression with timing of optic fissure fusion. Examining retina, and in particular optic fissure expression between 24 and 65hpf indicated that nid1a expression diminishes significantly by 36hpf while nid2a expression diminishes between 36 and 48hpf (Fig. 4B, Fig. S1D). By 48hpf, nid1a expression diminishes not only in the fissure, but also throughout the embryo while nid2a expression begins to corelate with the region of pharyngeal arches. In contrast, optic fissure and head expression of nid1b persists until 48hpf (Fig. 4B). By 56hpf all of the nidogen genes are no longer expressed in the optic fissure. These results indicate that optic fissure BMs contain nidogens 1a, 1b and 2a. Interestingly, our data also indicate that expression of nidogen orthologues may be temporally regulated in response to the initiation of optic fissure fusion.

2.5. Nidogen expression is uniquely regulated within the optic fissure basement membrane

When comparing and contrasting all of our optic fissure *in situ* hybridization data for laminin, collagen IV, perlecan and nidogen (Figs. 1–4) it becomes clear that during the course of optic fissure fusion only one core component of the basement membrane is transcriptionally responsive to the fusion process, that being nidogen (Figs. 4B and 5A). Nidogen expression is downregulated by 48hpf, with nid1a being downregulated as early as 36hpf, right at the predicted time of fusion initiation (Fig. 4 and A). All other BM components are still expressed in the fissure up to and/or later than 48hpf with perlecan expression persisting up to the conclusion of fissure fusion at 65hpf. These findings suggest that nidogen may be the first component of the BM to be remodeled or removed in order to enable wholesale disassembly of the BM thus facilitating epithelial fusion within the fissure. To test this hypothesis, we performed IHC to simultaneously detect laminin, a well-known marker for BM integrity, and nidogen. The nidogen antibody used was raised to mouse nidogen 1 and we therefore predict it detects nid1a and nid1b. We analyzed co-staining of laminin and nidogen from 22 to 48 hpf (Fig. 5B). At early time points, 22-36hpf, nidogen and laminin appear to co-localize in the BM and remain closely associated. However, by ~40-44hpf, a time when optic fissure fusion is predicted to be actively occurring and therefore BMs are being actively degraded or remodeled, within the central region of the fissure we begin to see regions of the BM having a reduction in nidogen signal prior to that of laminin (Fig. 5B). The absence of nidogen but persistence of laminin was not observed in every embryo examined (n = 3/10 embryos, at 42 and 44hpf), suggesting that BM remodeling is a highly dynamic event and soon after nidogen is removed so is laminin. However, we never observed the presence of nidogen in absence of laminin (n = 67 embryos between 32 and 56hpf). By the time fusion is complete, 48hpf or later, both signals are absent from the fusion sites. These results go hand in hand with our analysis of nidogen expression, where nidogen is the first BM component to be transcriptionally downregulated. This also suggests that nid1a and nid1b may in fact be the first components of the BM to be targeted in order to initiate disassembly, or remodeling, before the commencement of direct fusion of the optic fissure margins.

2.6. Nidogen is necessary for early retinal morphogenesis and optic fissure fusion

Previous studies of laminin subunits have pointed to a crucial function of the BM in shaping and maintaining the optic cup during early retinal morphogenesis (Bryan et al., 2016). To examine the functional role of nidogen during retinal morphogenesis and optic fissure fusion we performed morpholino injections for nid1a and/or nid1b in combination with Nid2a mutant analysis. Recent work from the Chen lab indicates that nid1a and 1b likely compensate each other upon loss of function (Zhu et al., 2017). As such, using morpholinos afforded us the opportunity to examine simultaneous loss of nid1a and 1b function (Fig. 6A). For nid2a we examined a mutant line sa15802 (ZIRC) which harbors a point mutation leading to a premature stop codon at amino acid 437 and subsequently exhibits nonsense mediated decay (Fig. 6B). Interestingly, examination of the nid2a mutant line did not reveal any observable phenotypes, even when generated as a maternal zygotic (Fig. 6B and data not shown). Nid2b was not functionally examined as it lacks optic fissure expression. Injection of nid1a or nid1b morpholinos into WT embryos resulted in a dose response of retinal and embryonic malformations (Fig. 6A). These included apparent developmental delays in the cranial

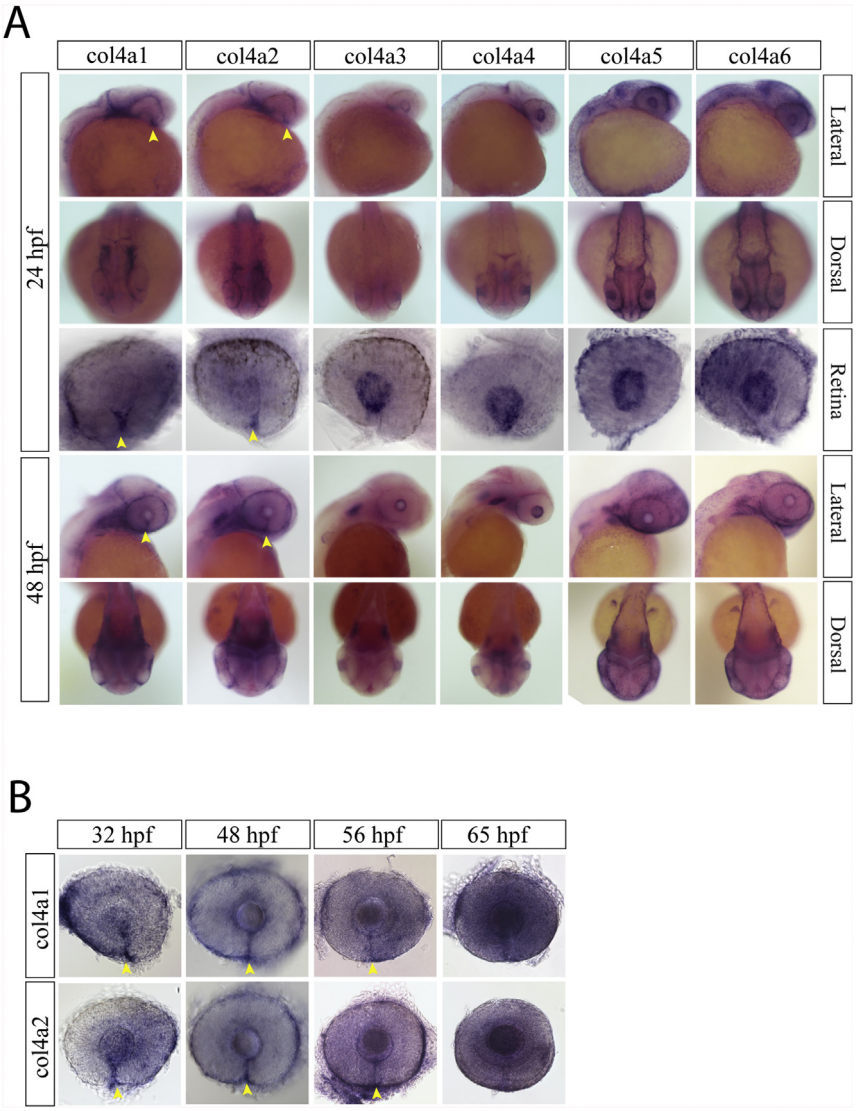

Fig. 3. Collagen IV expression during optic fissure formation and fusion. **A)** WISH for zebrafish collagen IV (col4) genes a1-a6 at 24hpf. At 24hpf, only collagen IV a1 and a2 had optic fissure expression (yellow arrow heads). Col4 a3-a6 were all detected in the retinal periphery and in the developing lens. **B)** WISH time course for col4 a1 and a2 expression from 24 to 65hpf. Both col4 a1 and a2 had detectable expression in the optic fissure up to 56hpf (yellow arrow heads).

regions (moderate) in combination with a decrease in overall embryo size (severe). Co-injection of both MOs had a synergistic effect leading to an increase in both moderate and severe phenotypes. Furthermore, injection of sub-effective doses of nid1a and nid1b MO into homozygous nid2a mutant embryos induced the highest proportion of severe phenotypes (Fig. 6C). This suggests that all three; nid1a, 1b and nid2a have potential compensatory function during early zebrafish development. Only moderately affected embryos were included in all subsequent functional studies. To visualize effects of nid1 loss of function on retinal morphogenesis we performed *in vivo* time lapse confocal microscopy using our retinal reporter line Tg[*rx3*:GFP] co-injected with nid1a/1b MOs. Nid2a−/− embryos injected with nid1a/1b MOs had too severe phenotypes to warrant detailed investigation of retinal morphogenesis. Starting at 20hpf we tracked retinal morphogenesis over 16 h (Fig. 6D, Movie 1 and 2). Already at 20hpf morphant embryos displayed a severely disorganized optic cup. As retinal development proceeded, morphant embryos did appear to complete optic cup formation but with several dire consequences. Throughout imaging we observed GFP + cells detaching from the retina, suggesting a lack of tissue integrity. In addition, even at 36 hpf, the retina has a very large gap between the two retinal lobes indicating a major extension of the N/T axis and unlikely ability to complete optic fissure fusion. Overall the morphant embryos displayed a very malformed and delayed retinal morphogenesis when compared to controls.

Supplementary video related to this article can be found at https://doi.org/10.1016/j.ydbio.2019.04.012.

Detailed analysis of nidogen loss of function during retinal morphogenesis was performed using IHC for laminin and in conjunction with the retinal reporter transgenic line Tg[*rx3*:GFP]. 24hpf embryos injected with nid1a, nid1b or both MOs were examined. Injection of both low and high dose of MO resulted in retinal malformation, in particular loss of symmetry in the retinal structure. This was evident with both laminin staining and the *rx3*:GFP signal (Fig. 7A). Higher doses (2 ng) of individual MOs or when co-injected resulted in a severely disorganized optic cup (Fig. 7B). We also observed regions of the retina where laminin deposition did not appear uniform or was absent. To quantify nidogen loss of function effects on retinal morphogenesis we measured both eye size (Fig. 7B) and eye symmetry (Fig. 7C) by calculating the nasal-temporal/dorsal ventral axis in morphant embryos with moderate phenotypes. Both nid1a and nid1b morphant embryos exhibited smaller eyes, ~16–20% reduction, with double morphants having significantly smaller eyes than either of the singles, up to a 24% reduction in size

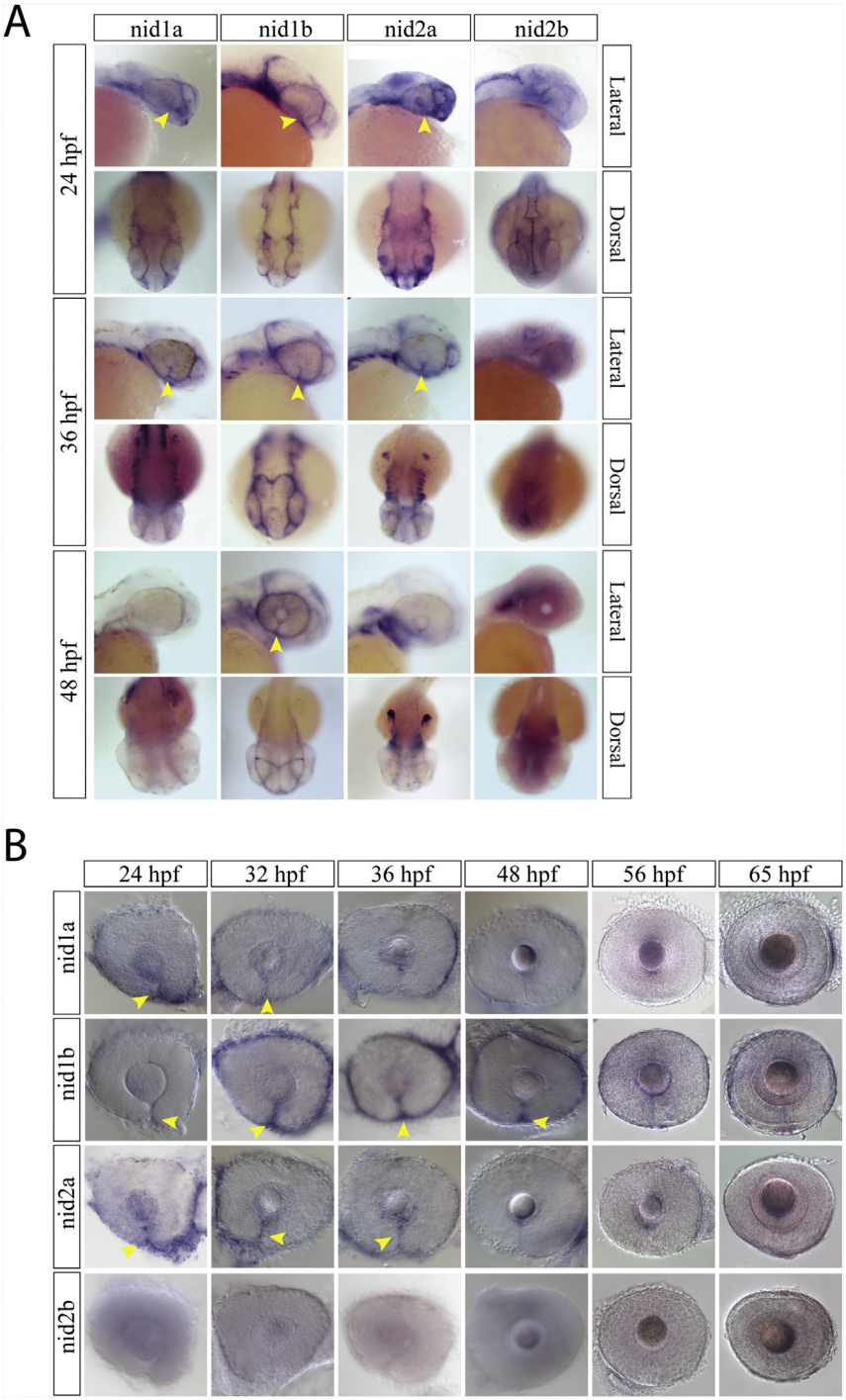

Fig. 4. Nidogen expression during optic fissure formation and fusion. **A)** WISH for zebrafish nidogen (nid) genes nid1a, nid1b, nid2a and nid2b at 24, 36 and 48hpf. At 24 and 36hpf nid1a, nid1b and nid2a were all expressed in the optic fissure (yellow arrow heads). Nid2b lack retinal expression between 24 and 48hpf. **B)** WISH time course for nid1a, 1b and 2a expression in the optic fissure (yellow arrow heads). Expression of nid1a and 2a is absent from the fissure by 48hpf, while nid1b persists past 48hpf but is absent by 56hpf.

(Fig. 7B). Decreased eye size was also associated with higher doses of the MOs. To determine a potential cause of smaller eyes we analyzed proliferation in nid1a/1b morphants by examining phospho-Histone H3 signal. At 24hpf we observed a significant reduction of retinal cells positive for PH3 when compared to controls (Fig. 7D). This reduction in proliferation could be a contributing factor to the decrease in eye size observed. As eye size decreased, we also observed an elongation of the NT axis in morphant embryos with the greatest effect also observed in double morphants and at higher MO concentrations (Fig. 7B) Elongation of the N/T axis ranged from 12 to 26% above that of controls. This was also evident in our *in vivo* time lapse imaging (Fig. 6C). To expand on these findings, we next examined N/T and D/V retinal patterning in morphant embryos. Whole mount *in situ* hybridization for FoxG1a (nasal), FoxD1 (temporal), Aldh1a2 (dorsal) and Vax2 (ventral) indicated that nidogen loss of function had specific effects on nasal-temporal retinal patterning. In particular, a shift of the dorsal domain, the aldh1a2 signal, in the nasal-ventral direction and a slight expansion of the dorsal domain, as observed with vax2 (Fig. 7E) Both the dorsal and ventral patterning abnormalities were observed at high penetrance (12/17 and 12/19 respectively). These findings indicate that morphogenesis of the retina, as well as D/V patterning, are significantly affected by the loss of nidogen (Fig. 7B–E).

As an alternative strategy for nidogen loss of function, we also generated a nidogen 1b dominant negative cDNA construct (nid1bDN) by removing the G3 domain. We predicted this construct would result in BM where nidogen would no longer be able to cross-link the other 3 core

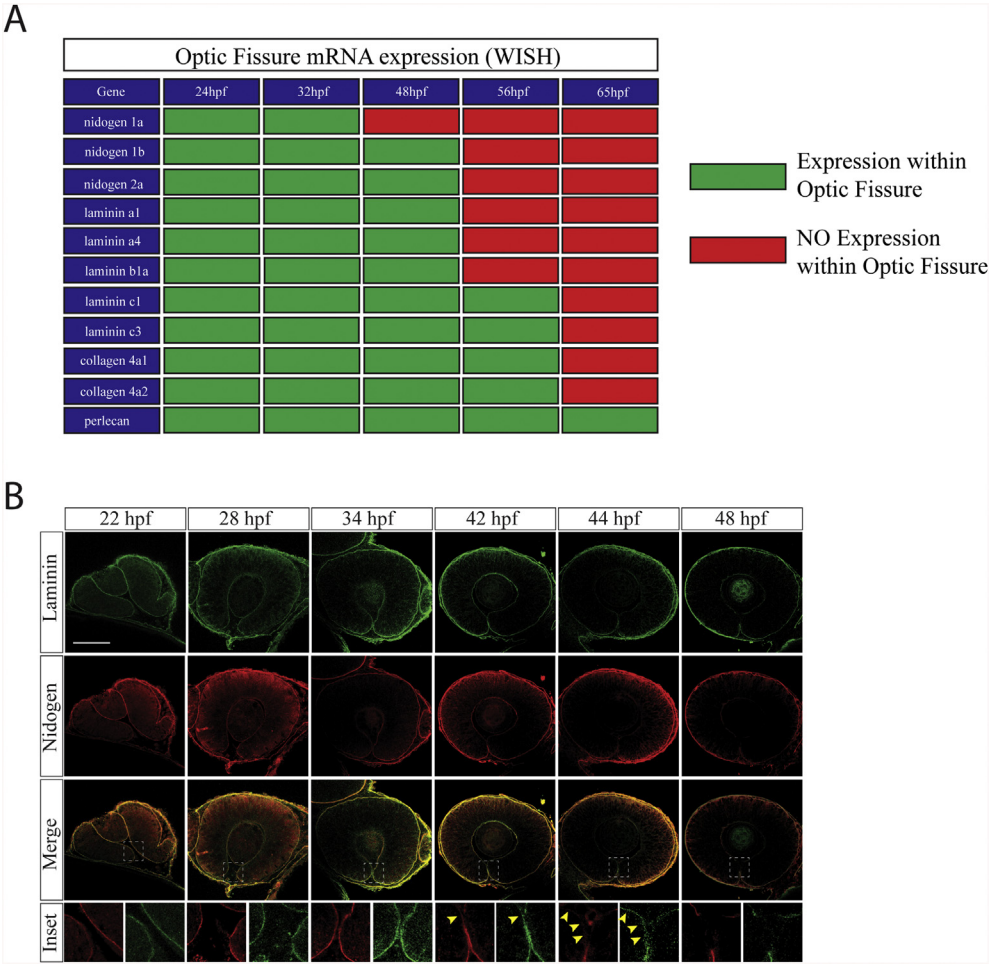

Fig. 5. Nidogen is down-regulated prior to laminin during optic fissure fusion. **A)** Summary of core basement membrane component expression within the optic fissure as observed by WISH (Figs. 1–4) between 24 and 65hpf. Green indicates expression (WISH signal), red indicates absence of expression (lack of WISH signal). **B)** Immunohistochemistry analysis for remodeling of laminin (green) and nidogen 1 (red) within the optic fissure during retinal morphogenesis (22-48hpf). At early time points, ~22-40hpf, laminin and nidogen signal is found to co-localize in the optic fissure BM. Starting at 42hpf nidogen signal in the optic fissure is reduced prior to that of laminin (yellow arrow heads). By 48hpf both laminin and nidogen are absent in the regions of the fissure where fusion has completed. Scale bar = 50 μm.

components and therefore weaken the structure. Injection of the nid1bDN mRNA resulted in malformation of the optic cup similar to what we observed in morphant embryos (Fig. S2). Taken together our data indicate that deposition of nidogen into the optic cup BM is essential for precise execution of retinal morphogenesis and maintenance of optic cup integrity. These findings are similar to what was observed in laminin mutant embryos.

Finally, we examined consequence of nidogen loss of function on optic fissure fusion. It was well documented that laminin mutant embryos experience a failure of fissure fusion and therefore a coloboma like phenotype (Lee and Gross, 2007). As such, we predicted that nidogen loss of function will results in similar outcomes. To examine fusion of the optic fissure we performed IHC for laminin at 72hpf in control and nid 1a/1b morphant embryos (Fig. 7F). When examining the central-distal region of the retina, control embryos exhibit little to no laminin or *rx3*:GFP signal in the region of the optic fissure as fusion has already completed. In contrast, more than 40% of nid1a/1b MO co-injected embryos retain laminin, and *rx3*:GFP signal in the region of the fissure outlining the two distinct lobes of the retina. This is an indication that BM remodeling has not completed, and that fissure fusion is either delayed or fails to initiate. As such, similar to laminin, nidogen is necessary during early development to ensure proper morphogenesis of the optic cup and subsequently the timely fusion of the optic fissure.

3. Discussion

The composition of the molecular machinery governing optic fissure fusion remains a black box. In our present study we begin to shed some light on this process by comprehensively analyzing the temporal expression of optic fissure basement membrane components. As such, our work is the first to define all of the core constituents of optic fissure basement membrane and observe an apparent order during to its remodeling. Based on our results we have concluded that optic fissure BMs are comprised of laminins a1, a4, b1, c1 and c3, perlecan, collagen 4a1 and 4a2 as well as nidogen 1a, 1b and 2a. Additionally, we have characterized the time course of their individual expression and determined that nidogen, in particular nidogen 1a and 2a is transcriptionally regulated in response to initiation of fissure fusion. While our study characterized the gross timing of core BM component expression, future studies will aim to decipher whether downregulation of nidogen expression has any distal-proximal temporal pattern and what is the corresponding transcriptional mechanism. Interestingly, we also observed that nidogen appears to be remodeled/removed in optic fissure BMs prior to that of laminin. Furthermore, nidogen loss of function appears to phenocopy laminin a1, b1 and c1 mutants, where retinal morphogenesis and subsequently optic fissure fusion are both impaired. Taken together we show that nidogen is a critical component of the retinal BM during optic fissure fusion and presents as a potential initial target of BM remodeling during fusion.

Limiting nidogen deposition in the zebrafish embryo via the use of morpholinos resulted in compromised BM structure and phenotypes similar to those observed in the murine model. Nidogen1 and 2 knockout mice have been shown to display BM defects in the heart, lung, and limbs resulting in perinatal lethality (Bader et al., 2005; Bose et al., 2006). These defects were observed to be a direct result of weakened BM integrity due to a decrease in the deposition of laminin, perlecan, and collagen IV. Additionally, knockout of nidogen 1 in mice has been reported to decrease the deposition of laminin γ1 resulting in a more

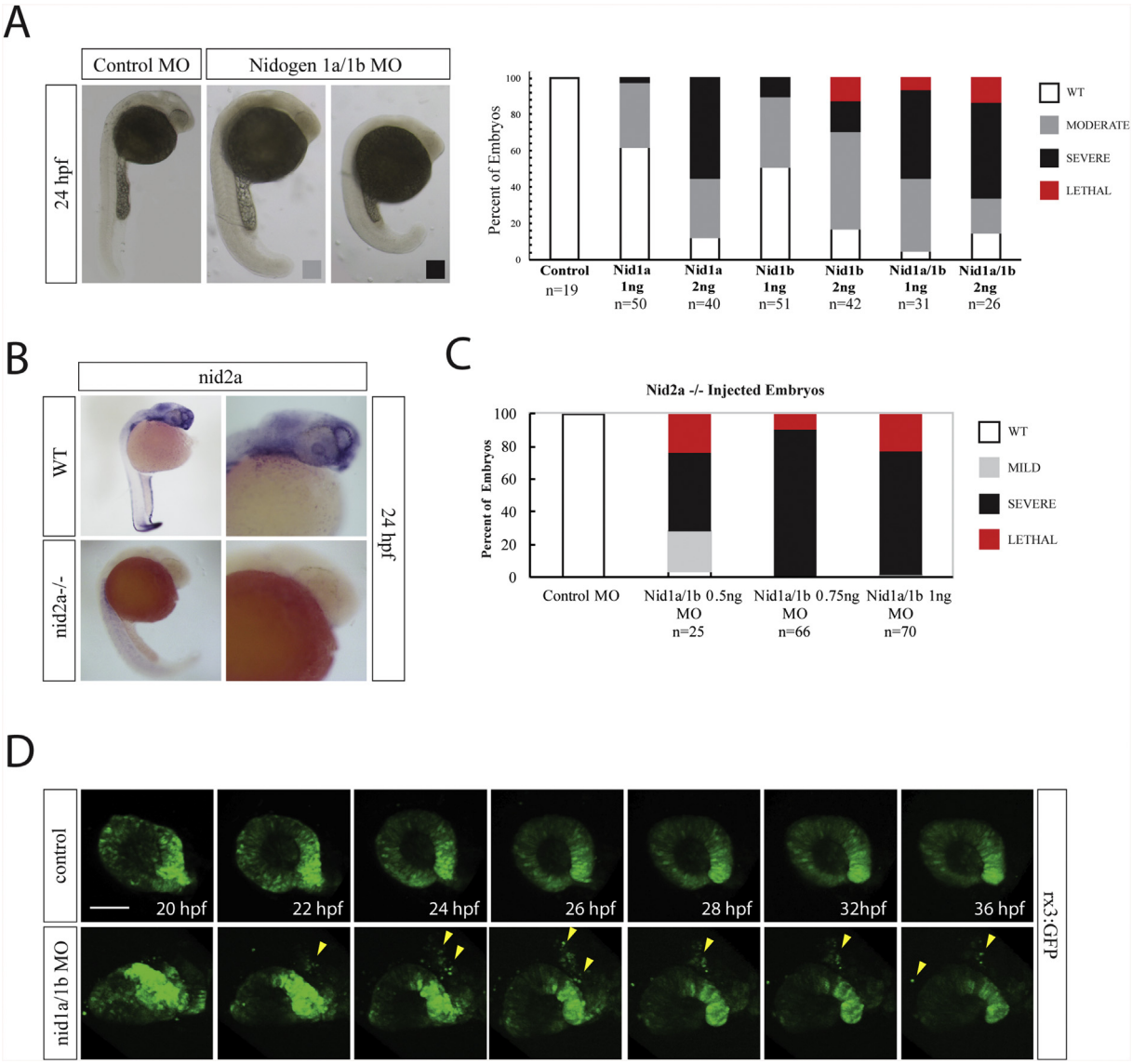

Fig. 6. Nidogen is required during retinal development. **A)** Nidogen 1a and 1b morpholino injection phenotypes at various concentrations and combinations. Moderate phenotypes (gray bar) included potential developmental delays but lacked overt morphological deficiencies. Severe phenotypes (black bar) included significant developmental delays and morphological deficiencies. Lethal phenotypes (red bar) included monster embryos and major developmental deficiencies. **B)** WISH for nid2a comparing expression in WT and nid2a^{sa15280} −/− embryos at 24hpf. Nid2a signal is completely absent in nid2a^{sa15280} −/− embryos. **C)** Nidogen 1a and 1b morpholino injections into nid2a^{sa15280} −/− embryos. Sub-effective doses of nid1a and nid1b MOs, 0.5 or 0.75 ng each, resulted in up to 80% of embryos exhibiting severe or lethal phenotypes. At 1 ng the injections resulted in exclusively severe or lethal phenotypes. **D)** *In vivo* real time imaging of *rx3*:GFP embryos co-injected with nid1a and nid1b morpholinos. 3D stacks were collected every 10min for 16 h. Compared to control, nid1 morphants display a disorganized optic cup, a significant delay in the formation of opposing retinal lobes, an elongation of the N/T axis and delamination of retinal progenitor cells (yellow arrowheads). Scale bar = 50 μm.

punctate and less uniform BM compared to controls (Baranowsky et al., 2010). Unfortunately, as far as we know coloboma or any ocular phenotypes were not examined in nid1, nid2 or double KO mice. Future analysis of ocular phenotypes of these animals would be very useful.

In addition to studies of nidogen mutants, there have been reports showing the ablation of other basement membrane components resulting in adverse effects on ocular development. For example, loss of laminin a1 has been observed to disrupt zebrafish vertebrate optic cup morphogenesis (Bryan et al., 2016). The authors documented multiple structural abnormalities in zebrafish embryos lacking laminin a1 including defects in focal adhesion, invagination, and optic stalk constriction. On a macroscopic level they observed morphogenic phenotypes similar to nidogen morphants including a misshapen lens, and smaller eyes. The authors also noted patches of dying cells they hypothesized could be a result of cells losing contact with the basement membrane and entering into apoptosis via anoikis. Similarly, in our live imaging study of nidogen morphants, we observed *rx3*:GFP + cells which appear to lose contact with the basement membrane and subsequently detach from the eye (Fig. 6D). In addition, we observed a decrease in retinal proliferation in nid1a/1b morphants (Fig. 7D). Previous studies examining laminin b1 and laminin c1 revealed basement membrane defects affecting both the developing eye and notochord of zebrafish (Lee and Gross, 2007; Parsons et al., 2002). Both mutants showed smaller eyes and lens abnormalities similar to those observed in our nidogen morphants. Furthermore, these embryos also displayed shortened body axis comparable to nidogen morphant embryos. Together, it is clear that BM integrity is essential for proper embryonic development and that loss of even one core component can robustly alter ocular morphogenesis.

Our study suggests that nidogen may act as the first target of BM remodeling during optic fissure fusion. We hypothesize that there are two

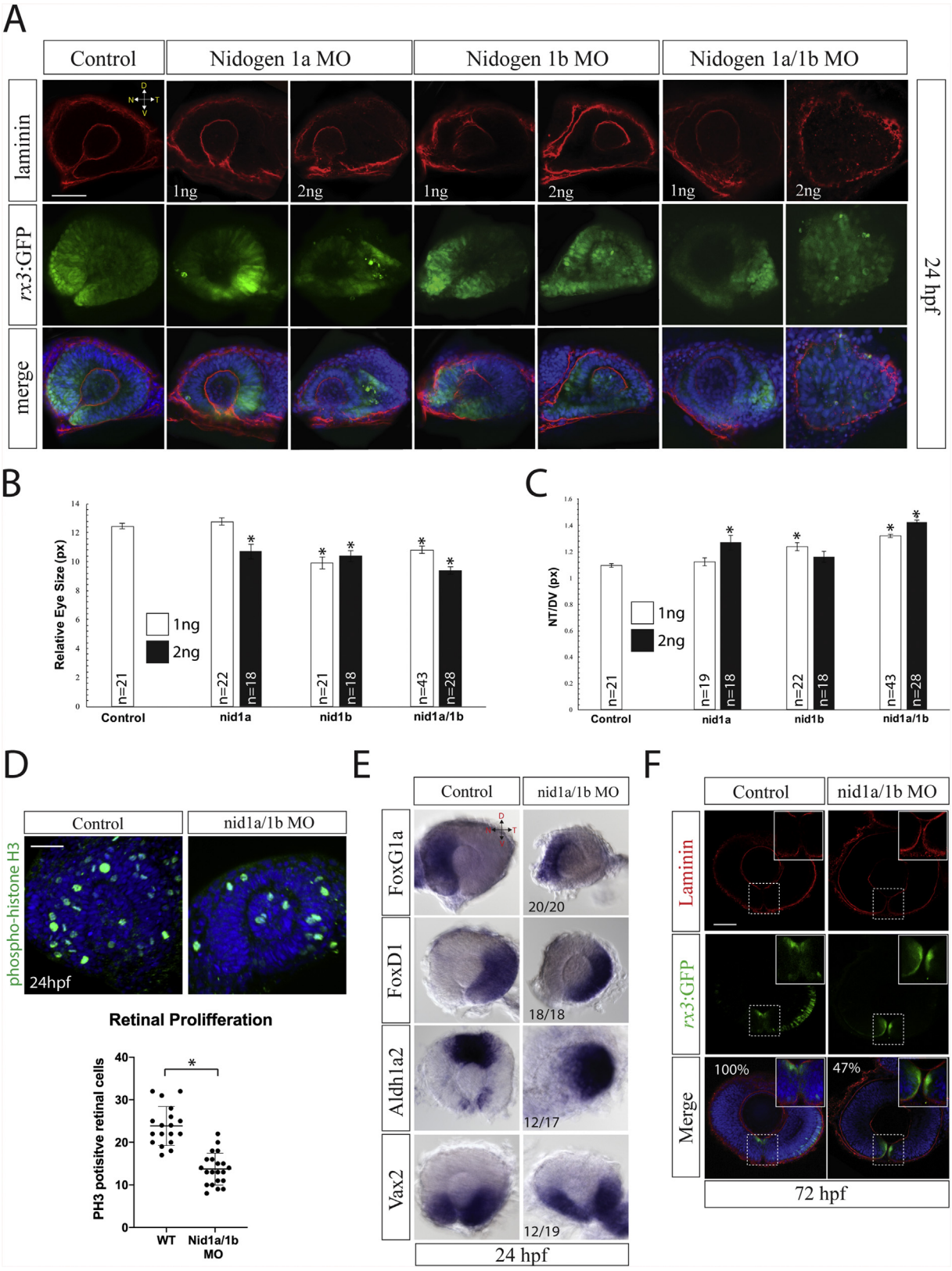

(caption on next page)

Fig. 7. Nidogen is essential for accurate retinal morphogenesis. **A)** Retinal phenotypes in 24hpf nid1 morphant *rx3*:GFP (green) expressing embryos were characterized using laminin IHC (red), and DAPI (blue). Representative single confocal sections are depicted. Retinal shape is moderately disrupted at low morpholino concentrations (1 ng) with most severe effects observed in double morphant embryos (2 ng). Laminin deposition appears to be mildly affected upon co-injection of nid1a and 1b MO at 2 ng 40–50 embryos were examined for each treatment. Scale bar = 50 μm. **B)** Quantification of relative retinal size observed in 24hpf morphant embryos. Significantly smaller eyes were observed upon injection of either nid1a or nid1b morpholinos, with the smallest resulting from co-injection of nid1a and 1b morpholinos. Student T-tests were conducted between control and all treatment groups for each parameter measured. * = $p < .005$. **C)** Quantification of retinal shape in 24hpf nidogen morphant embryos. Injection of nid1a or nid1b results in an extended NT axis, with co-injection having a synergistic effect. Student T-tests were conducted between control and all treatment groups for each parameter measured. * = $p < .05$. **D)** Phospho-histoneH3 (PH3) staining (green) at 24hpf in control and nid1a/1b co-injected embryos. 3D reconstructions are displayed. PH3+ cell counts from individual embryos analyzed are graphed. DAPI is shown in blue. WT n = 19, Nid1a/1b MO n = 23. *p = .0001, Student T-test. Scale bar = 50 μm. **E)** WISH for temporal, foxG1a, nasal, foxD1, ventral, vax2 and dorsal, aldh1a2 in nid1a/nid1b morphant retinas at 24hpf. WT and morphant embryo eyes were dissected, mounted and imaged. Nid1a/1b morphant eyes show no significant effects on nasal/temporal patterning, while ventral domains appear shifted temporally and dorsal regions expanded. **F)** Examination of optic fissure fusion at 72hpf via laminin (red) IHC in *rx3*:GFP (green) expressing morphant embryos. Inset (dashed square) displays high magnification of the optic fissure. Single confocal planes of the central-distal region of the fissure are depicted. Results reveal the persistence of laminin signal in 47% (n = 41 control, n = 27 nid1a/1b MO, p = .0001) of 72hpf morphant fissures, a time when control embryos have already completed fusion and removed laminin. Scale bar = 50 μm.

potential modes in which the structural disassembly of the BM through the removal of nidogen facilitates optic fissure fusion. The first predicts that the removal of nidogen from the BM results in the exposure of proteolytic sites in the core BM components of laminin, collagen IV or perlecan. Specifically, removal of nidogen leads to a disrupted basement membrane architecture allowing for the subsequent liberation of newly exposed epitopes in other basement membrane components. In this model, matrix metalloproteases which recognize these newly exposed epitopes now have the ability to efficiently remodel the other core basement membrane components. A second, and alternative model predicts that in the absence of nidogen, BM integrity is compromised allowing for the extension of cellular protrusions involved in fusion, such as lamelopodia and filopodia. Ultimately, reducing the biomechanical strength of the BM allows for the necessary positioning of epithelial sheets and subsequent fusion. Interestingly, this possibility has recently been documented in the study of anchor cell invasion (Laura et al., 2019). Finally, it is not only possible, but likely, that these two proposed modes work in concert to enable fusion. Future studies using Atomic Force Microscopy to analyze the degree of optic fissure BM integrity in the absence of nidogen function would potentially answer these questions.

Regulation of nidogen function during fissure fusion appears to be regulated at both the transcriptional and posttranslational level. An examination of other BM remodeling events provides evidence that gene expression does have the ability to play consequential roles in altering BM structure. During heart failure for example, the myocardial BM is significantly remodeled which has been hypothesized to alter cellular shape and function ultimately resulting in decreased performance (Kim et al., 2016). A study examining the variance of gene expression of ischemic failing and non-failing hearts in human tissue suggests that the differential expression of BM components, including the down-regulation of nidogen and laminin, do indeed effect BM morphology (Kim et al., 2016). Transmission electron microscopy revealed, amorphous disrupted BMs in failing hearts known to have lower levels of nidogen and laminin gene expression. Our results suggest, that the integrity of the optic fissure BM may decrease via a similar developmental mechanism in which the expression of nidogen is purposely reduced.

Posttranslational targeting and removal of nidogen in the optic fissure via endogenous proteases provides a direct route for dismantling the BM. Interestingly, nidogen is the most proteolytically sensitive BM component, and is therefore uniquely capable of acting as an initiating factor during BM remodeling (Mayer et al., 1993, 1995; Sires et al., 1993). BM remodeling is predominantly predicted to involve the function of MMP, ADAM and ADAMTS proteases. However, to date only two such proteases, MMP2 and ADAMTS16, have been associated with function during optic fissure fusion (Cao et al., 2018; Tsuji et al., 2018). Unfortunately, direct targets within the optic fissure for ADAMTS16 or MMP2 have yet to be identified. Several proteases have shown to have affinity for nidogen cleavage *in vitro*, including MMP18 and 19 and as such will need to be a topic of future studies to determine whether they play functional roles in optic fissure BM remodeling (Alexander et al., 1996; Titz et al., 2004; Tonge et al., 2013). Lastly, recent work detailing the expression pattern of genes associated with the optic fissure indicates that expression of MMP24 and MMP23bb is upregulated during fissure fusion suggesting these proteases may also be playing a role in BM remodeling (Richardson et al., 2019).

In conclusion, our study has catalogued the core components of the BM expressed during optic fissure fusion and informed on their regulation. Armed with this information we can better prepare to investigate the molecular mechanisms governing optic fissure BM remodeling and subsequently fusion of the optic fissure.

4. Materials and methods

4.1. Zebrafish and embryo maintenance

Zebrafish were maintained using husbandry procedures approved by University of Kentucky IACUC committee. AB and TL strains were used as wild-type, *rx3*:GFP transgenic line (Holly et al., 2014; Rembold et al., 2006) was used to visualize retinal morphogenesis. Embryos were kept at 28.5 °C in E3 embryo media. Nid2a^{sa15280} embryos were purchased from ZIRC. RFLP analysis was conducted by amplifying the region of gDNA with the nidogen2a mutation using the forward primer: 5′-TGATCC-TATTACTCGAC AGATAATAAAG3-'and the reverse: 5′-CGTTTGGCAGGCAGTGGCGGC-3'. The resultant 460bp amplicon was digested with ApeKI (NEB) which would recognize and digest the mutated allele sequence but not the WT allele. Nid2a^{sa15280} homozygous fish were viable and maintained in a homozygous $^{sa15280/as15280}$ state.

4.2. Whole-mount in situ hybridization (WISH)

Whole-mount *in situ* hybridization was performed as previously described (Holly et al., 2014). WISH was performed on 50 + embryos in 2–3 distinct experiments for each time point and each probe. DIG labeled RNA probes were generated using PCR with T7 promoter sequence included in the reverse primer and subsequently transcribed using T7 polymerase (Roche). Primer sequences can be found in Supplementary Table 1. Images were captured using a Nikon Digital sight DS-Fi2 camera and Elements software. Dissected eyes from 24, to 65hpf embryos were mounted in 70% glycerol and imaged under DIC using a Nikon TiE compound microscope equipped with a 20X (0.95NA) objective and Elements software. Image adjustment was performed using Adobe Photoshop.

4.3. Immunofluorescence (IHC)

Dechorionated embryos were fixed with 4% PFA in PBS at room temperature for 3 h and washed with PBST 3 times for 10 min. Embryos were then permeabilized with Proteinase K, 30 μg/mL 15 min for 24 hpf, 50 μg/mL 30 min for 48 hpf and 75 μg/mL 30 min for 72 hpf, washed 3 times in PBST for 5 min and blocked overnight at 4 °C with 10% sheep

serum, 0.8% Triton X-100 and 1% BSA in PBS. Primary mouse anti-laminin antibody (3H11-c DSHB – 1:100) and rabbit anti-nidogen (Abcam 14511- 1:100) in blocking buffer (1% sheep serum, 1% BSA and 0.8% Triton X-100 in PBS) were incubated overnight at 4 °C and washed 5 times in PBST for 10 min. Secondary antibodies, donkey anti-rabbit Alexa Fluor® 555 (Molecular Probes – 1:1000) or mouse anti-GFP Daylight 488 (Rockland – 1:500) and DAPI 1:1000, were incubated for 1 h at room temperature in the dark. Primary rabbit anti-laminin antibody (ThermoFisher – 1:100) was used for IHC in morphant embryo analysis. The embryos were washed 5 times in PBST for 10 min and visualized using a Nikon C2+ confocal microscope equipped with a 40X (1.15NA) water immersion objective. Embryos were embedded in 1% low melting point agarose on glass bottom 35 mm dishes (Fluorodish, World Precision Instruments). Images were captured using Nikon Elements software and adjusted for brightness, contrast and positioning using Adobe Photoshop. All images were adjusted in similar fashion and according to standard image processing guidelines.

4.4. Phospho-histone H3 (PH3) proliferation assay

24hpf embryos were subjected to whole mount IHC as described above. Rabbit anti-PH3 antibody (Millipore 06–570, 1:100) was incubated O/N at 4 °C. Alexa Fluor® 488 anti rabbit secondary antibody (Molecular Probes, 1:1000 + DAPI) was incubated at RT for 2 h. Embryos were mounted in low gelling agarose in 35 mm Fluorodishes and imaged using a C2+ Nikon confocal microscope with a 20X, 0.95NA objective. ~90 μm stacks were collected using a 3 μm step size. 3D projections were generated and PH3 positive cells were counted from within the retina. Statistical analysis was conducted using Microsoft Excel Data Package. Student T-tests were conducted between all treatment groups for each parameter measured. The significance cutoff was $p < .005$.

4.5. Morpholino injections

Translation blocking Morpholinos were obtained from Gene Tools, LLC and used to knock down the expression of nidogen1a and nidogen1b. The following morpholinos were used in this study: Control MO: 5′-CCTCTTACCTCAGTTACAATTTATA-3′, nidogen1a: 5′-GTGCCGACCCA-TATCCAGTCCCAAA-3′, and nidogen1b: 5′-CGGCATCTTCCCCAGG-TAGTCAGAC-3'. Standard control morpholinos were used as controls at matching concentrations. Morpholino concentrations were determined by a dose response of concentration from 0.5 to 8 ng. Concentrations resulting in >90% survivability and absence of gross morphological phenotypes were selected. For analysis, injected morpholino concentrations were 1 ng and 2 ng of nid1a and 1b independently, and 1 ng and 2 ng of nid1a/1b. Morpholino concentrations injected into *nid2a−/−* embryos were nid1a/1b at 0.5 ng, 0.75 ng and 1 ng. Statistical analysis was conducted using Microsoft Excel Data Package. Student T-tests were conducted between all treatment groups for each parameter measured. The significance cutoff was $p < .005$.

4.6. Live imaging analysis

Live imaging of nidogen1a/1b morphant embryos was conducted using a Nikon C2+ confocal microscope equipped with at 20X (0.95NA) water immersion objective. 2 ng of nidogen1a and 1b or control morpholino were injected into 1 cell stage of *rx3*:GFP positive embryos. 20hpf Embryos were imbedded in 1% low gelling agarose in 1-inch glass bottomed Flourodish cell culture dishes (World Precision Instruments) and covered in embryo media, 3-amino benzoic acidethylester (tricaine) to anaesthetize the embryos and 1-phenyl 2-thiourea (PTU) to inhibit pigmentation. Z-stacks 75 μm thick with a step size of 2.5 μm were captured over the course of 16 h at 10 min intervals. ($n = 3$ control embryos and $n = 4$ nid1a/1b MO injected embryos) The ambient temperature was kept at 28 °C. The time lapse data was reconstructed in 4D using Elements software. Image adjustment for brightness, contrast and positioning was done using Adobe Photoshop. All images were adjusted in similar fashion and according to standard image processing guidelines.

4.7. Eye size measurements

Embryos injected with morpholino were fixed in 4% paraformaldehyde. Eye images were captured using a Nikon Digital sight DS-Fi2 camera equipped on a Nikon SMZ800 stereomicroscope. Following image capture, ImageJ software was used to quantify parameters of the morphant embryo eyes. To obtain a measurement of eye size, the area of the eye, measured in pixels (px) was divided by the length of the embryo (px) (from the distal tip of the head to the end of the tail) to normalize for variable embryo size. To obtain a measurement of eye shape, the embryos were positioned laterally, and the length of the nasal/temporal (NT) axis was measured (px) as well as the dorsal/ventral (DV) axis was measured (px) and the ratio of the two (NT/DV) was calculated. Statistical analysis was conducted using Microsoft Excel Data Package. Student T-tests were conducted between all treatment groups for each parameter measured. The significance cutoff was $p < .005$.

4.8. Dominant negative mRNA injection

Truncated nidogen 1b constructs were generated using PCR (primers found in Supplementary Table 1), cloned into pCS2+8 (Addgene) and confirmed via sequencing. mRNA was generated using the Sp6 mMessage mMachine kit (Ambion). Embryos were injected with 200 pg, 300 pg, and 350 pg of mRNA.

Funding

This work was supported by the Knights Templar Eye Foundation Career Starter Grant Awarded to JK. Famulski, 2016–2018.

Appendix A. Supplementary data

Supplementary data to this article can be found online at https://doi.org/10.1016/j.ydbio.2019.04.012.

References

Alexander, C.M., et al., 1996. Rescue of mammary epithelial cell apoptosis and entactin degradation by a tissue inhibitor of metalloproteinases-1 transgene. J. Cell Biol. 135 (6 Pt 1), 1669–1677.
Aumailley, M., 2013. The laminin family. Cell Adhes. Migrat. 7 (1), 48–55.
Aumailley, M., et al., 1989. Binding of nidogen and the laminin-nidogen complex to basement membrane collagen type IV. Eur. J. Biochem. 184 (1), 241–248.
Aumailley, M., et al., 1993. Nidogen mediates the formation of ternary complexes of basement membrane components. Kidney Int. 43 (1), 7–12.
Bader, B.L., et al., 2005. Compound genetic ablation of nidogen 1 and 2 causes basement membrane defects and perinatal lethality in mice. Mol. Cell Biol. 25 (15), 6846–6856.
Baranowsky, A., et al., 2010. Impaired wound healing in mice lacking the basement membrane protein nidogen 1. Matrix Biol. 29 (1), 15–21.
Barishak, Y.R., 1992. Embryology of the eye and its adnexae. Dev. Ophthalmol. 24, 1–142.
Bernstein, C.S., et al., 2018. The cellular bases of choroid fissure formation and closure. Dev. Biol. 440 (2), 137–151.
Bonnans, C., Chou, J., Werb, Z., 2014. Remodelling the extracellular matrix in development and disease. Nat. Rev. Mol. Cell Biol. 15 (12), 786–801.
Bose, K., et al., 2006. Loss of nidogen-1 and -2 results in syndactyly and changes in limb development. J. Biol. Chem. 281 (51), 39620–39629.
Brown, K.L., et al., 2017. Building collagen IV smart scaffolds on the outside of cells. Protein Sci. 26 (11), 2151–2161.
Bryan, C.D., Chien, C.B., Kwan, K.M., 2016. Loss of laminin alpha 1 results in multiple structural defects and divergent effects on adhesion during vertebrate optic cup morphogenesis. Dev. Biol. 416 (2), 324–337.
Cao, M., et al., 2018. Metalloproteinase Adamts16 is required for proper closure of the optic fissure. Invest. Ophthalmol. Vis. Sci. 59 (3), 1167–1177.
Chang, L., et al., 2006. Uveal coloboma: clinical and basic science update. Curr. Opin. Ophthalmol. 17 (5), 447–470.
Chung, A.E., Durkin, M.E., 1990. Entactin: structure and function. Am. J. Respir. Cell Mol. Biol. 3 (4), 275–282.
Gestri, G., et al., 2018. Cell behaviors during closure of the choroid fissure in the developing eye. Front. Cell. Neurosci. 12, 42.

Gregory-Evans, C.Y., et al., 2004. Ocular coloboma: a reassessment in the age of molecular neuroscience. J. Med. Genet. 41 (12), 881–891.
Holly, V.L., et al., 2014. Sfrp1a and Sfrp5 function as positive regulators of Wnt and BMP signaling during early retinal development. Dev. Biol. 388 (2), 192–204.
Hornby, S.J., Ward, S.J., Gilbert, C.E., 2003. Eye birth defects in humans may be caused by a recessively-inherited genetic predisposition to the effects of maternal vitamin A deficiency during pregnancy. Med. Sci. Monit. 9 (11), HY23–H26.
Hutter, H., et al., 2000. Conservation and novelty in the evolution of cell adhesion and extracellular matrix genes. Science 287 (5455), 989–994.
Hynes, R.O., Zhao, Q., 2000. The evolution of cell adhesion. J. Cell Biol. 150 (2), F89–F96.
James, A., et al., 2016. The hyaloid vasculature facilitates basement membrane breakdown during choroid fissure closure in the zebrafish eye. Dev. Biol. 419 (2), 262–272.
Khoshnoodi, J., Pedchenko, V., Hudson, B.G., 2008. Mammalian collagen IV. Microsc. Res. Tech. 71 (5), 357–370.
Kim, E.H., et al., 2016. Differential protein expression and basal lamina remodeling in human heart failure. Proteonomics Clin. Appl. 10 (5), 585–596.
Laura, C., Kelly, Q.C., Rodrigo Caceres, Eric Hastie, Schindler, Adam J., Jiang, Yue, Matus, David Q., Plastino, Julie, Sherwood, David R., 2019 Feb 11. Adaptive F-actin polymerization and localized ATP production drive basement membrane invastion in the absence of MMPs. Dev. Cell 48 (3), 313–328.
Lee, J., Gross, J.M., 2007. Laminin beta1 and gamma1 containing laminins are essential for basement membrane integrity in the zebrafish eye. Invest. Ophthalmol. Vis. Sci. 48 (6), 2483–2490.
Li, S., et al., 2003. The role of laminin in embryonic cell polarization and tissue organization. Dev. Cell 4 (5), 613–624.
Liu, C., et al., 2016. A secreted WNT-ligand-binding domain of FZD5 generated by a frameshift mutation causes autosomal dominant coloboma. Hum. Mol. Genet. 25 (7), 1382–1391.
Mayer, U., et al., 1993. Sites of nidogen cleavage by proteases involved in tissue homeostasis and remodelling. Eur. J. Biochem. 217 (3), 877–884.
Mayer, U., et al., 1995. Binding properties and protease stability of recombinant human nidogen. Eur. J. Biochem. 227 (3), 681–686.
Parsons, M.J., et al., 2002. Zebrafish mutants identify an essential role for laminins in notochord formation. Development 129 (13), 3137–3146.
Paulsson, M., et al., 1987. Structure of low density heparan sulfate proteoglycan isolated from a mouse tumor basement membrane. J. Mol. Biol. 197 (2), 297–313.
Reis, L.M., Semina, E.V., 2015. Conserved genetic pathways associated with microphthalmia, anophthalmia, and coloboma. Birth Defects Res. C Embryo Today 105 (2), 96–113.
Rembold, M., et al., 2006. Individual cell migration serves as the driving force for optic vesicle evagination. Science 313 (5790), 1130–1134.
Richardson, R., et al., 2019. Transcriptome profiling of zebrafish optic fissure fusion. Sci. Rep. 9 (1), 1541.
Saint-Geniez, M., D'Amore, P.A., 2004. Development and pathology of the hyaloid, choroidal and retinal vasculature. Int. J. Dev. Biol. 48 (8–9), 1045–1058.
Sanyanusin, P., et al., 1995. Mutation of PAX2 in two siblings with renal-coloboma syndrome. Hum. Mol. Genet. 4 (11), 2183–2184.
Sanyanusin, P., et al., 1995. Mutation of the PAX2 gene in a family with optic nerve colobomas, renal anomalies and vesicoureteral reflux. Nat. Genet. 9 (4), 358–364.
Sires, U.I., et al., 1993. Degradation of entactin by matrix metalloproteinases. Susceptibility to matrilysin and identification of cleavage sites. J. Biol. Chem. 268 (3), 2069–2074.
Smith, S.M., et al., 2007. Heparan and chondroitin sulfate on growth plate perlecan mediate binding and delivery of FGF-2 to FGF receptors. Matrix Biol. 26 (3), 175–184.
Stoll, C., et al., 1997. Congenital eye malformations in 212,479 consecutive births. Ann. Genet. 40 (2), 122–128.
Sztal, T., et al., 2011. Characterization of the laminin gene family and evolution in zebrafish. Dev. Dynam. 240 (2), 422–431.
Take-uchi, M., Clarke, J.D., Wilson, S.W., 2003. Hedgehog signalling maintains the optic stalk-retinal interface through the regulation of Vax gene activity. Development 130 (5), 955–968.
Timpl, R., 1993. Proteoglycans of basement membranes. Experientia 49 (5), 417–428.
Titz, B., et al., 2004. Activity of MMP-19 inhibits capillary-like formation due to processing of nidogen-1. Cell. Mol. Life Sci. 61 (14), 1826–1833.
Tonge, D., et al., 2013. Axonal growth towards Xenopus skin in vitro is mediated by matrix metalloproteinase activity. Eur. J. Neurosci. 37 (4), 519–531.
Tsao, T., et al., 1990. Characterization of the basement membrane glycoprotein entactin synthesized in a baculovirus expression system. J. Biol. Chem. 265 (9), 5188–5191.
Tsuji, N., et al., 2012. Organogenesis of mild ocular coloboma in FLS mice: failure of basement membrane disintegration at optic fissure margins. Exp. Eye Res. 94 (1), 174–178.
Tsuji, N., et al., 2018. Macrophage-associated gelatinase degrades basement membrane at the optic fissure margins during normal ocular development in mice. Invest. Ophthalmol. Vis. Sci. 59 (3), 1368–1373.
Yurchenco, P.D., 1990. Assembly of basement membranes. Ann. N. Y. Acad. Sci. 580, 195–213.
Yurchenco, P.D., Schittny, J.C., 1990. Molecular architecture of basement membranes. FASEB J. 4 (6), 1577–1590.
Zhu, P., et al., 2017. Short body length phenotype is compensated by the upregulation of nidogen family members in a deleterious nid1a mutation of zebrafish. J. Genet. Genom. 44 (11), 553–556.
Zoeller, J.J., et al., 2008. A central function for perlecan in skeletal muscle and cardiovascular development. J. Cell Biol. 181 (2), 381–394.